European Journal of Mechanics / B Fluids 83 (2020) 73–85

Contents lists available at ScienceDirect

European Journal of Mechanics / B Fluids

journal homepage: www.elsevier.com/locate/ejmflu

Aerodynamic performance improvement of a pitching airfoil via a synthetic jet

Junjie Wang [b,c], Jie Wu [a,b,c,d,*]

[a] State Key Laboratory of Mechanics and Control of Mechanical Structures, Nanjing University of Aeronautics and Astronautics, Yudao Street 29, Nanjing, Jiangsu 210016, China
[b] Department of Aerodynamics, Nanjing University of Aeronautics and Astronautics, Yudao Street 29, Nanjing, Jiangsu 210016, China
[c] Key Laboratory of Unsteady Aerodynamics and Flow Control, Ministry of Industry and Information Technology, Nanjing University of Aeronautics and Astronautics, Yudao Street 29, Nanjing, Jiangsu 210016, China
[d] College of Aerospace Engineering, Shenyang Aerospace University, Daoyi South Street 37, Shenyang, Liaoning 110136, China

ARTICLE INFO

Article history:
Received 7 January 2020
Received in revised form 15 April 2020
Accepted 21 April 2020
Available online 23 April 2020

Keywords:
Dynamic stall
Flow control
Synthetic jet
Low Reynolds number
Compressible flow

ABSTRACT

The aim of the present work is to control the dynamic stall of a pitching NACA0012 airfoil and improve its aerodynamic performance by using a synthetic jet in a low Reynolds number compressible flow for use in prospective applications, such as flights on Mars and in the stratosphere. A recently developed variable correction-based immersed boundary method is employed to predict the complex flow fields. A sinusoidal function is selected to fulfill the periodic jet. Compared with the situation without control, the use of a synthetic jet can obtain a significant improvement of the aerodynamic performance of the pitching airfoil. Based on the numerical results, adjusting the phase angle to trigger the suction time of the synthetic jet at a large angle of attack can obtain the best lift increment and drag reduction. Additionally, in a small variation range, a larger jet momentum coefficient can produce better aerodynamic performance. However, when the jet momentum coefficient increases up to some fixed value, the enhancement is weakened. Furthermore, placing the jet at the leading edge is more conducive to improving the aerodynamic performance. Finally, the higher the Mach number, the worse the control effect of the synthetic jet.

1. Introduction

Recently, some evidence has suggested that there is liquid water on Mars; thus, exploring the planet Mars has become more popular. However, the drawbacks of the Mars Rovers include the low speed and the narrow field of view. Thus, using autonomous flying vehicles to further the surface exploration could be a good choice in the future, and they can also act as scouts for the Rovers. In contrast to the atmosphere on Earth, the Martian atmosphere is rarefied and mostly consists of carbon dioxide (96%) and has a low density ($\rho \approx 0.014$ kg m^{-3}). Meanwhile, the speed of sound ($a \approx 238$ m s^{-1}) is relatively low [1]. Therefore, a typical flying vehicle designed for Mars exploration would operate in a low Reynolds number, compressible flow regime. Munday et al. [2] numerically and experimentally investigated the flow past a triangular airfoil of Martian flying vehicles at Reynolds numbers of 3000 and 10 000 and Mach numbers of 0.15 and 0.5. Another problem is related to the energy supply. Compared to the weather on Earth, there are often sandstorms and hurricanes on Mars, and the wind on Mars is also stronger. Although solar energy is used on Mars, the solar panels may be covered by sandstorms. Some studies have suggested that small, lightweight wind turbines can work under Martian atmosphere conditions. However, both Martian flying vehicles and wind turbines (especially at the blade tip) will operate in a low Reynolds number, compressible flow regime. The low Reynolds number flow will promote both flow separation and high viscous drag [1]. Dynamic stall, which is one of the most complex aerodynamic issues, presents a unique combination of unsteady effects, nonlinear flow and strong vortex interaction. Dynamic stall plays a significant role in various aerodynamic applications, including the manoeuverability of the Martian aircraft and the wind turbine blade. Although many works have been conducted to control the dynamic stall under the earth's atmosphere, it is valuable to reinvestigate this issue in a low Reynolds number, compressible flow regime.

Tseng and Cheng [3] investigated the vortex interaction of incompressible flow over a pitching airfoil with different reduced frequencies at a high Reynolds number (2.5×10^6). It was found that the mechanism of delaying the stall came from the formation

* Corresponding author at: State Key Laboratory of Mechanics and Control of Mechanical Structures, Nanjing University of Aeronautics and Astronautics, Yudao Street 29, Nanjing, Jiangsu 210016, China.
E-mail address: wuj@nuaa.edu.cn (J. Wu).

https://doi.org/10.1016/j.euromechflu.2020.04.009
0997-7546/

Nomenclature

C_D	Drag coefficient
C_L	Lift coefficient
C_μ	Momentum coefficient
c	Chord length, m
e_t	Total energy, J
$\mathbf{f}$	General force term, N
H	Jet width, m
h	Plunging position, m
h_0	Plunging amplitude, m
k	Dimensionless reduced frequency
L	Jet location, m
Ma	Mach number
p	Pressure, Pa
$\dot{q}$	General heat addition term, J
Re	Reynolds number
t	Time, s
U_{sj}	Jet velocity amplitude, m/s
U_∞	Freestream velocity, m/s
$\mathbf{u}$	Fluid velocity, m/s
u_{sj}	Jet velocity, m/s
α	Angle of attack, °
θ	Fluid temperature, K
λ	Thermal conductivity
$\prod$	The tensor of viscous constraints
ρ	Fluid density, kg/m^3
ϕ_{sj}	Jet phase angle
ω	Pitching frequency
ω_{sj}	Jet frequency
Γ	Circulation

of the leading edge vortex (LEV), which played an important role in the dynamic stall. Furthermore, the low-pressure area of the LEV provided the extra lift force. However, the lift force would drop dramatically once the shedding of LEV takes place. For the dynamic condition, the separation of the LEV from the airfoil occurred later compared with the static condition, but the development of the trailing edge vortex (TEV) could cause the recirculation region of the LEV to collapse. Consequently, the lift force would decrease significantly when the TEV forms. Hamid and Kyung [4] obtained similar conclusions. Furthermore, the secondary and tertiary LEVs or TEVs have been investigated carefully. After the dynamic stall occurred, the secondary LEV provided a lift peak in the post-stall substituting for the primary LEV. During the down-stroke, the flow structure around the airfoil became very complicated, and the secondary and tertiary TEVs would interact with the secondary and tertiary LEVs. Therefore, the lift production would decrease and the hydrodynamic loads would fluctuate.

The characteristics of the dynamic stall are influenced by the reduced frequency of the pitching motion, the freestream flow condition, the Reynolds number, the Mach number, and the foil shape. McAlister et al. [5] and McCroskey et al. [6] investigated the dynamic stall of a pitching NACA0012 foil with different reduced frequencies by using the experimental method. Visbal [7] analyzed the onset of the dynamic stall of a pitching SD7003 foil at a Reynolds number of 5×10^5. Visbal [8] also examined the influence of compressibility on the dynamic stall and observed that the supersonic flow region starts to grow as the angle of the attack increases. Due to the severe shock-boundary-layer interaction, the separation near the shock location starts to spread both upstream and downstream. Guo et al. [9] studied the dynamic stall phenomena under different situations (Mach number varies from 0.2 to 0.6 and Reynolds number varies from 5000 to 20,000). Thus, the dynamic stall has been described in detail, which could be helpful for controlling it.

Niu and Chang [10] indicated that the vortices would almost dominate the contributions of the aerodynamics during the entire stroke. The reduction and the fluctuation of the lift could be improved by controlling the vortices. Zhong et al. [11] controlled the dynamic stall on a vertical axis wind turbine with the installation of a small rod in front of the leading edge of the foil. Their results revealed that the counter-rotating vortices shedding from the rod continuously transmit kinetic energy into the boundary layer of the airfoil, which could prevent the formation of a dynamic stall vortex. Therefore, the flow separation from the foil could be avoided and the lift force could be improved. Wolfgang and Berend [12] used an airfoil with an appropriate deformation to avoid a strong vortex. As a result, the propulsion efficiency of the flapping airfoil was improved. However, one of the most popular active flow control techniques might be the synthetic jet (SJ) control with zero-mass-flux. Tang et al. [13] utilized a SJ to control the large-scale separation on the airfoil and increased the maximum lift by 48% compared with the uncontrolled flow. A Genetic Algorithm was employed in their work to optimize the combination of the SJ parameters, including the velocity amplitude, frequency and angle with respect to the wall. A similar control method was applied by Zhao et al. [14] with the use of dual-jets. Moreover, the location of the SJ is also an important control parameter, and the SJ should be placed near the flow separation point. Generally speaking, the main principle of SJ control is to add the kinetic energy into the boundary layers of the airfoils to suppress the formation of vortices. Therefore, the frequency of the SJ was typically very high to achieve the continuous kinetic energy in the previous studies [13,14]. Meanwhile, the dynamic stall control by the SJ worked at a high Reynolds number O(10^6) in these studies. It will be difficult to break the vortex structure when such an SJ control method is employed in the situation of a low Reynolds number. Therefore, further investigation is needed when using the SJ for dynamic stall control when the aircrafts, helicopter rotors and wind turbines operate in the Martian atmosphere.

Although the stronger SJ working in the low Reynolds number flow can overcome the viscous effect to suppress the vortex induced vibration of a circular cylinder [15], an SJ with a higher speed might not yet work well for the oscillating airfoil. Wang and Tang [16] used an in-phase SJ pair to improve the aerodynamic performance of an elliptic airfoil heaving with fixed pitching angles in a low Reynolds number incompressible flow. In their study, the SJ pair operated at the same heaving motion frequency. With some appropriate phase angles, the suction and blowing strokes of the SJ pair could effectively enhance the aerodynamic performance. Their control principle is different from [13,14]. High-frequency jets were used in [13,14] to inject kinetic energy into the boundary layers of airfoils to suppress the formation of vortices. In contrast, a low-frequency jet was used in [16] to control the main vortex to prevent it from shedding prematurely and causing more small vortices and backflow areas. At a low Reynolds number, the vortex force is often much larger than the added mass force and viscous force [16]. The generation and evolution of vortices around the airfoil play a key role in the production of aerodynamic forces, and hence, the manipulation of these vortices can significantly change the aerodynamic forces. The choice of high or low frequency jets is mainly based on the Reynolds number. Considering the low Reynolds number environment in the current work, the high-frequency SJ may not work as well as in [13,14].

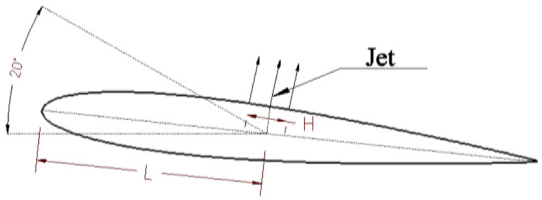

Fig. 1. The pitching airfoil and the jet on the upper surface.

Summarizing the main findings mentioned above, the Martian atmosphere results in a low Reynolds number, compressible flow regime, and controlling the dynamic stall at this regime is important. The generation and evolution of vortices around the boundary play a key role in the production of aerodynamic forces during the dynamic stall. Suppressing [13,14] or controlling [16] them can improve the aerodynamic performance. At a low Reynolds number, low frequency jets may obtain better control effects. This study aims to control the dynamic stall of a pitching airfoil in a low Reynolds number, compressible flow regime to obtain a larger lift and smaller drag or a higher lift–drag ratio. Similar to the previous work [16], an SJ with the same pitching motion frequency will be employed to control the dynamic stall in this work. A NACA0012 airfoil pitching around the quarter-chord will be considered, which is the same as the work in Ref. [9] ($Ma = 0.4$, $\mathrm{Re} = 5000$). The effects of the phase angle, momentum coefficient, jet location and compressibility of fluid on the aerodynamic performance of the airfoil will be investigated in detail.

2. Problem description and numerical method

2.1. Problem description

In this study, a NACA0012 airfoil pitching around the quarter-chord is simulated, and the angle of attack varies according to the following:

$$\alpha(t) = 10^{\circ}\left[1 - \cos(\omega t)\right] \tag{1}$$

where ω is the pitching frequency, which can be calculated from the dimensionless reduced frequency as follows:

$$k = \frac{\omega c}{2U_{\infty}} \tag{2}$$

where c is the chord length of the airfoil, and U_{∞} is the freestream velocity.

To improve the aerodynamic performance of the pitching airfoil, a synthetic jet is implemented on the upper surface of the airfoil. The time-dependent velocity of the SJ can be expressed as follows:

$$u_{sj} = U_{sj}\sin(\omega_{sj}t + \phi_{sj}) \tag{3}$$

where U_{sj} is the amplitude of the jet velocity, ω_{sj} is the jet frequency, which is equal to the airfoil's pitching frequency ω in the present work, and ϕ_{sj} is the phase angle of the jet. Additionally, the direction of the jet velocity is always perpendicular to the airfoil's surface, as shown in Fig. 1. H is the width of the jet and L is the location of the jet center from the leading edge. Because of the sinusoidal variation of the jet velocity, no net mass is added [13,14,16]. The momentum coefficient quantifying the SJ strength and power consumption can be written as follows [16]:

$$C_{\mu} = \frac{8U_{sj}^2 H}{9U_{\infty}^2 c} \tag{4}$$

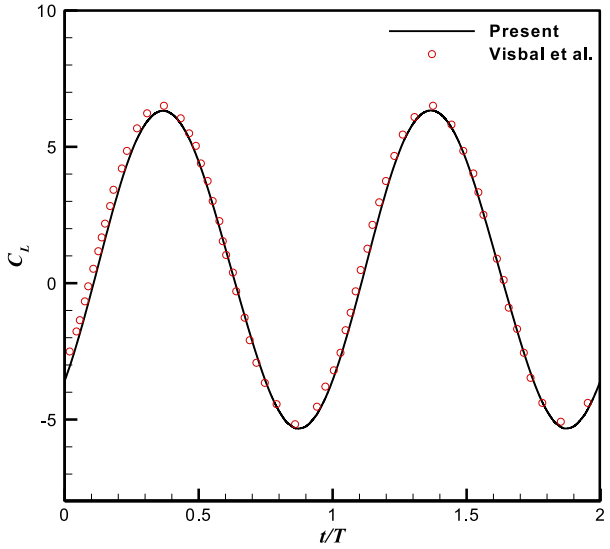

Fig. 2. Lift coefficient C_L versus normalized time t/T.

In addition, the Mach number Ma and Reynolds number Re are defined as $Ma = \frac{U_{\infty}}{\sqrt{\gamma R\theta_{\infty}}}$ and $\mathrm{Re} = \frac{\rho_{\infty}U_{\infty}c}{\mu}$, respectively, where γ is the specific heat ratio, which kept constant at 1.4 in the present work, R is the specific gas constant, θ_{∞} is the freestream temperature, ρ_{∞} is the freestream density, and μ is the dynamic viscosity. The lift coefficient, drag coefficient, and pressure coefficient are defined as $C_L = \frac{F_L}{(1/2)\rho_{\infty}U_{\infty}^2 c}$, $C_D = \frac{F_D}{(1/2)\rho_{\infty}U_{\infty}^2 c}$, and $C_p = \frac{p_B - p_{\infty}}{(1/2)\rho_{\infty}U_{\infty}^2}$, respectively, where F_L is the lift force, F_D is the drag force, and p_B is the pressure on the boundary of the airfoil.

2.2. Governing equation and prediction step

To simulate the viscous compressible flow over the NACA0012 airfoil, a recently proposed variable correction-based immersed boundary method [17] is adopted in this work. Both stationary and moving bodies could be simulated by using this method [17,18], and all the results compared well with the data in the literature. In this method, there are mainly two steps, i.e., prediction and correction.

For the viscous compressible flow, the governing equations can be written as follows:

$$\frac{\partial \rho}{\partial t} + \nabla\cdot(\rho\mathbf{u}) = 0 \tag{5a}$$

$$\frac{\partial(\rho\mathbf{u})}{\partial t} + \nabla\cdot(\rho\mathbf{u}\mathbf{u}) = -\nabla p + \nabla\cdot\prod + \mathbf{f} \tag{5b}$$

$$\frac{\partial(\rho e_t)}{\partial t} + \nabla\cdot(\rho e_t\mathbf{u}) = -\nabla\cdot(p\mathbf{u}) + \nabla\cdot\left(\prod\mathbf{u}\right) + \nabla\cdot(\lambda(\theta)\nabla\theta) + \dot{q} \tag{5c}$$

where ρ is the fluid density, $\mathbf{u}$ is the fluid velocity, p is the pressure, $\prod$ is the tensor of viscous constraints, $\mathbf{f}$ is the general force term, λ is the thermal conductivity, θ is the fluid temperature, and $\dot{q}$ is the general heat addition term. In addition, e_t is the total energy, which includes kinetic energy and internal energy. As the perfect gas is considered here, the equation of state $p = \rho R\theta$ is adopted.

In the prediction step, the immersed boundary effect is ignored temporarily, and the governing equations (5a)–(5c) without the general force $\mathbf{f}$ and heat addition $\dot{q}$ terms are solved to obtain the intermediate variables (density ρ^*, velocity $\mathbf{u}^*$, temperature θ^* and pressure p^*). All the intermediate variables are computed with *rhoCentralFoam* in OpenFoam (https://openfoam.org/).

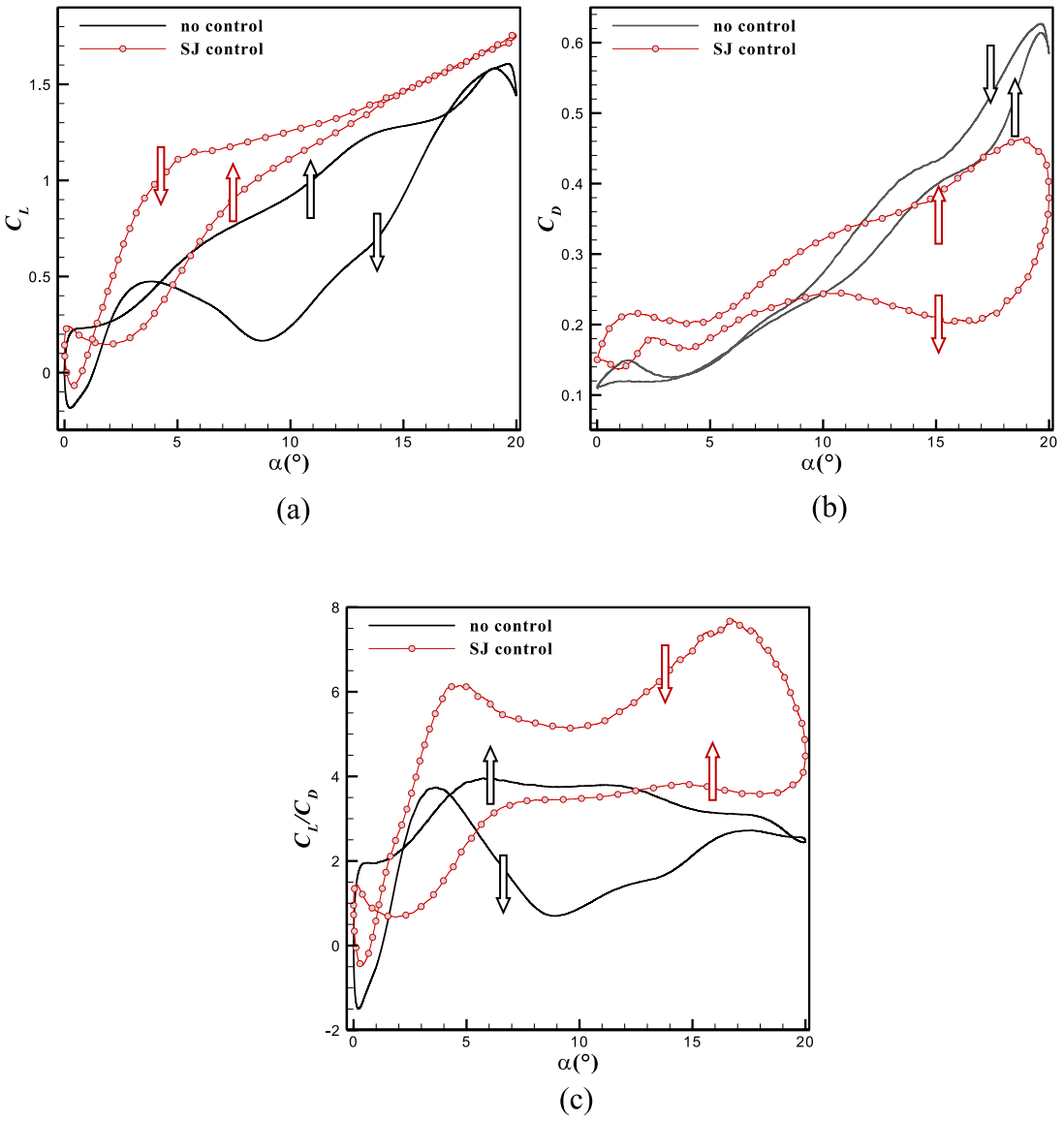

Fig. 3. Comparison of the aerodynamic force coefficients with and without synthetic jet control: (a) lift coefficient, (b) drag coefficient, and (c) the ratio of the lift coefficient to the drag coefficient varying with the angle of attack.

Particularly, the *rhoCentralFoam* solver in OpenFoam is the semi-implicit segregated density-based solver with the Kurganov–Tadmor divergence scheme for compressible flows, which is a second-order central scheme and can capture discontinuity/shock features well.

2.3. Boundary conditions and variable correction

To take the immersed boundary effect into account, boundary conditions need to be implemented. In this study, the no-slip boundary condition and the isothermal boundary condition are considered. In the immersed boundary method employed, thus, they are implemented in the correction step.

First, the fluid velocity correction $\delta\mathbf{u}$ can be calculated by the following:

$$\delta\mathbf{u} = \sum \delta\mathbf{u}_B \delta^B = \sum \delta\mathbf{u}_B D\left(\mathbf{x} - \mathbf{X}\right) \Delta s \tag{6}$$

where $\mathbf{x}$ is the location of the fluid point and $\mathbf{X}$ is the location of the boundary point, $\delta\mathbf{u}_B$ is the boundary velocity correction, $D\left(\mathbf{x} - \mathbf{X}\right)$ is the delta function, and Δs is the arc length of the boundary. $\delta\mathbf{u}_B$ can be calculated via the no-slip boundary condition, and then the corrected fluid velocity is achieved via $\mathbf{u}^{n+1} = \mathbf{u}^{*,n} + \delta\mathbf{u}$, where $\mathbf{u}^{*,n}$ is the intermediate velocity calculated in the prediction step. It should be noted that Eq. (6) is the summation over all the boundary points.

Second, the temperature can be corrected through the implementation of the isothermal boundary condition. After that, the density and pressure can be updated according to the continuity equation and equation of state, respectively. More details about the correction step can be found in Ref. [17].

2.4. Validation of the numerical method

The current immersed boundary method has been well applied to simulate compressible flow over stationary and moving bodies. To further validate its capability for dynamic stall problems, a simulation of the flow around a plunging SD7003 airfoil is performed. The Reynolds number based on the airfoil chord length is 10 000, and the Mach number is set as 0.2. The SD7003 airfoil plunges with a static angle of attack $\alpha_0 = 4°$, and the

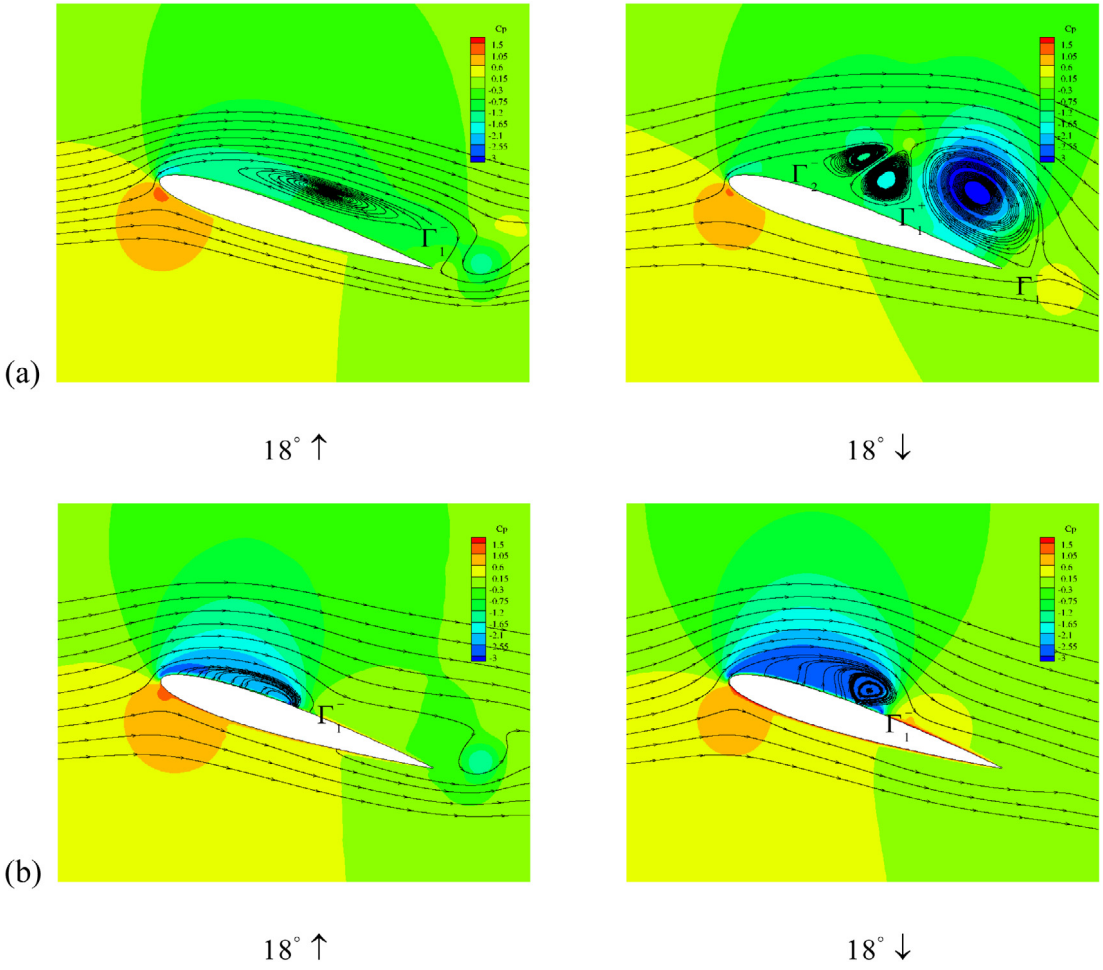

Fig. 4. Pressure coefficient contours and streamline at two instants: (a) uncontrolled and (b) synthetic jet control.

plunging motion is given as follows:

$$h(t) = h_0 \sin(2kU_\infty t/c) \tag{7}$$

where the plunging amplitude is $h_0 = 0.05c$, and the reduced frequency of the plunging motion is $k = 3.93$. The computational domain is $[-20c, 30c] \times [-20c, 20c]$ with a grid size of 481×281, and the number of Lagrangian points (i.e., boundary points) on the airfoil is 400. A uniform mesh with mesh spacing $\Delta h = 0.005c$ is used around the airfoil.

Fig. 2 shows the time evolution of the lift coefficient. The same problem has been simulated by Visbal et al. [19]. It is shown that the present result agrees well with that in the previous study [19]. Therefore, the current method can be convinced when it is applied to dynamic stall problems.

3. Flow control and analyses

3.1. Basic movement and SJ control

In the following simulations, the reduced frequency of the pitching NACA0012 airfoil is fixed at $k = 0.5$. Meanwhile, the airfoil operates in the low Reynolds number compressible flow with $Ma = 0.4$ and $\mathrm{Re} = 5000$. The computational domain is $[-15c, 25c] \times [-15c, 15c]$, which is covered by rectangular grids with the grid size of 451×301, and a uniform mesh with mesh spacing $\Delta h = 0.005c$ is used around the airfoil. The pitching axis is located at (0, 0), and there are 400 Lagrangian points distributed along the airfoil surface.

To check the effect of the synthetic jet on the aerodynamic performance of the pitching airfoil, a synthetic jet with $C_\mu = 0.068$ ($U_{sj} = 0.875U_\infty$, $H = 0.1c$), $\phi_{sj} = 0.5\pi$ and $L = 0.5c$ is added to the upper surface of the airfoil. For the case without a synthetic jet, it is noted that the aerodynamic force coefficients start to change periodically from the 8th pitching period. Thus, this result is set as the benchmark, and it will be used as an initial field to simulate the cases with the synthetic jet control.

Fig. 3 provides an overview of the aerodynamic force coefficients varying with the angle of attack α with and without SJ controls. Specially, the arrow represents the airfoil's pitching direction (upstroke or downstroke). Figs. 4 and 5 show the pressure coefficient around the airfoil. They will be used to investigate the cause of the aerodynamic changes and the control mechanism. For the case without control, the change of the lift coefficient during the upstroke is approximately linear with the increase of α until the dynamic stall appears. From Fig. 3(a), it is found that the lift coefficient drops at approximately $\alpha = 18°\uparrow$, which means the dynamic stall has occurred [9]. From Fig. 4(a), the vortex Γ_1^- is dragged long and gradually leaves the upper surface of the airfoil at $\alpha = 18°\uparrow$. During the downstroke, the C_L drops greatly compared with that during the upstroke at the same α. In the meanwhile, the C_D increases greatly at a large α and it is a little larger than that during the upstroke (as shown in Fig. 3(b)). Therefore, the ratio of the lift coefficient to the drag coefficient C_L/C_D is decreased not only at a large α but also during almost the whole downstroke (as shown in Fig. 3(c)). From Fig. 4(a), it is observed that even at the same angle of attack, the flow fields on

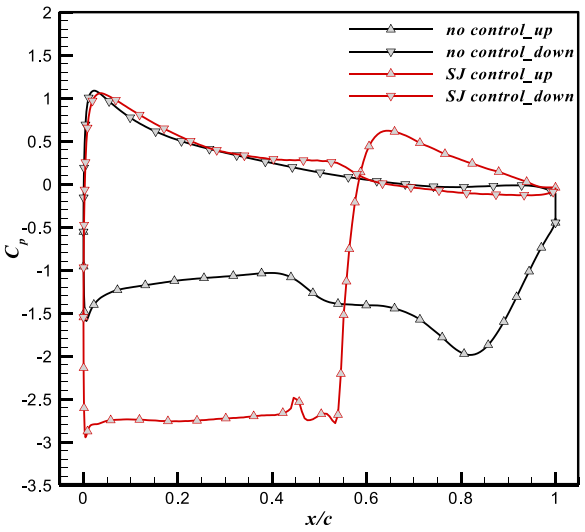

Fig. 5. Pressure coefficient along the upper and lower surface at 18°↓ with and without synthetic jet control.

Table 1
Comparison of the time-averaged lift and drag coefficients with and without synthetic jet control.

	$\overline{C_L}$	$\overline{C_D}$	$\overline{C_L/C_D}$
Without control	0.787	0.318	2.277
With SJ control	1.037	0.263	3.774

the airfoil upper surface during the up and down strokes are very different. At $\alpha = 18°\downarrow$, the main vortex Γ_1^- detaches from the upper surface of the airfoil and more vortices Γ_1^+, Γ_2^- form after the vortex Γ_1^-. Vortex Γ_1^- shedding also takes away the huge low pressure area. Consequently, C_L drops greatly during the whole downstroke. Therefore, poor aerodynamic performance occurs. This phenomenon has been explained in detail in the previous works [3,4].

However, when the synthetic jet is employed, the aerodynamic performance can be improved significantly. From Fig. 3(a), it is found that the variation of C_L is approximately linear with the increase of α during the whole upstroke, even at a large α. From Fig. 4(b), with $\alpha = 18°\uparrow$, the vortex Γ_1^- is intercepted by the jet in the middle of the airfoil upper surface and is firmly attached to the airfoil surface. The vortex Γ_1^- provides a low pressure field at the leading edge. At $\alpha = 18°\downarrow$, there is little change in the flow field on the airfoil upper surface compared with $\alpha = 18°\uparrow$. The vortex Γ_1^- and low pressure regions increase and the pressure coefficient decreases, which is definitely beneficial for improving the aerodynamic performance. When the downstroke begins, the C_L shows almost no difference compared with that during the upstroke at a large α, which is opposite to the uncontrolled case. Furthermore, the C_L is also higher than that without control during the downstroke at a small α; thus, the time-averaged lift coefficient $\overline{C_L}$ is increased from 0.787 to 1.037, as listed in Table 1. As shown in Fig. 3(b), compared with the uncontrolled case, the C_D is decreased clearly at a large α, especially during the downstroke. Even if there is a higher drag at a small α, the time-averaged drag coefficient $\overline{C_D}$ is still reduced from 0.318 to 0.263. Therefore, C_L/C_D can be improved greatly at a large α and during the whole downstroke period, as shown in Fig. 3(c). Fig. 5 provides an overview of C_p along the upper and lower surfaces at 18°↓ with and without synthetic jet control. At this instant, there is almost no difference between controlling and not controlling C_p along the airfoil lower surface. However, the distribution of C_p along the airfoil upper surface is consistent with that shown in Fig. 4. With an SJ, the pressure along the leading half of the airfoil's lower surface decreases significantly. Without an SJ, the vortex Γ_1^- is about to take away the large low-pressure area, and the low-pressure area generated by the newly formed vortices is obviously insufficient. It can be predicted that once the vortex Γ_1^- completely falls off, the lift coefficient will drop sharply, which is also consistent with the performance shown in Fig. 3.

The results in Fig. 3 indicate that the dynamic stall has been effectively controlled and the aerodynamic performance has been improved by using the synthetic jet. Although the momentum coefficient C_μ used is very small compared with that in the previous work [13–16], the behaviors of C_L and C_D have clearly been improved, which implies that the mechanism of the control method used here may be different from that in Ref. [14], where the vortices were blown away from the airfoil's surface. Based on the above results and analysis, the purpose of the jet used here is to maintain the leading edge vortex formed during the upstroke phase. The leading edge vortex Γ_1^- is an advantage brought by the dynamic stall, and the occurrence of stall is delayed in the upstroke phase [3]. Such a vortex was employed in the previous work to continue to exert its advantages in the downstroke phase. Controlling the position and timing of this vortex will effectively improve the aerodynamic performance. This control principle is similar to Ref. [16]. Thus, more details about the mechanism of SJ control and parametric analyses will be presented in the next sections.

3.2. Effect of the jet phase angle

To investigate the effect of the phase angle of the jet, eight values of "-ϕ_{sj} are chosen from 0 to 2π",- with a constant interval of $\pi/4$. The other parameters are fixed, i.e., $C_\mu = 0.068$ ($U_{sj} = 0.875U_\infty$, $H = 0.1c$) and $L = 0.5c$. Fig. 6 provides the time-averaged lift coefficient, drag coefficient and the ratio of the lift coefficient to the drag coefficient ($\overline{C_L}$, $\overline{C_D}$ and $\overline{C_L/C_D}$) at different SJ phase angles ϕ_{sj}. In the figure, the horizontal dashed lines represent $\overline{C_L}$, $\overline{C_D}$ and $\overline{C_L/C_D}$ without control, which can be called the baselines. As seen from the figure, $\overline{C_L}$ is above the baseline when $\phi_{sj} \leq \pi$. However, when $\phi_{sj} > \pi$, $\overline{C_L}$ decreases and is below the baseline. On the other hand, $\overline{C_D}$ is always below the baseline for all the values of ϕ_{sj} considered. In particular, the drag reduction is not obvious when ϕ_{sj} equals to 0 or π, while when ϕ_{sj} is 0.5π or 1.5π, $\overline{C_D}$ is reduced greatly. However, when ϕ_{sj} is 0.25π or 0.5π, $\overline{C_L/C_D}$ is significantly greater than in the other cases. A larger $\overline{C_L/C_D}$ means better aerodynamic performance.

To investigate the lift increment and drag reduction principles, three phase angles ($\phi_{sj} = 0.5\pi$, π, 1.5π) are chosen, and the results are compared with those of the uncontrolled case. Fig. 7 plots the dimensional velocity of the SJ u_{sj}/U_{sj} varying with the pitching angle, from 0° to 20° (upstroke) and 20° to 0° (downstroke). The direction of u_{sj} is perpendicular to the airfoil's surface, and a positive value represents blowing while a negative value is suction. Considering 6 instants, i.e., $\alpha = 18°\uparrow$, 20°, 18°↓, 15°↓, 10°↓, and 5°↓, the corresponding vertical dashed lines are marked in Fig. 7. Then, the suction or blowing behavior can be easily identified at these instants. Fig. 8 shows the vorticity contours around the airfoil at these instants, and Fig. 9 provides the variations of the drag and lift coefficients with respect to the angle of attack at different phase angles.

According to the results in Section 3.1, it is known that the aerodynamic performance is poor without SJ control. As shown in Fig. 8(a), the generated vortices detach from the upper surface of the airfoil. As a result, the negative pressure region along the upper surface of the airfoil is destroyed. For the convenience of the investigation, the main vortex Γ_1^- is considered, which is

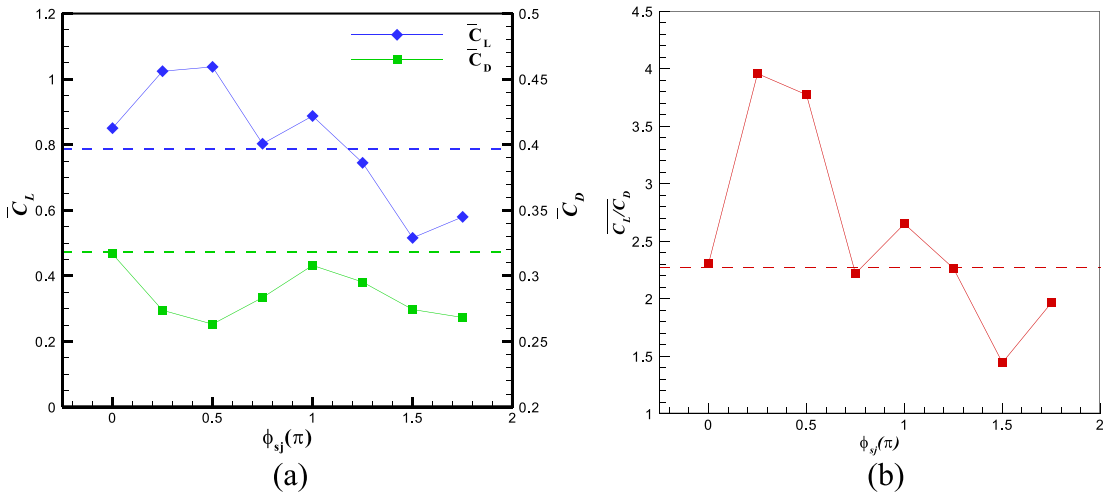

Fig. 6. Time-averaged (a) lift and drag coefficients ($\overline{C_L}$ and $\overline{C_D}$) (b) the ratio of the lift coefficient to the drag coefficient ($\overline{C_L/C_D}$) at different SJ phase angles ϕ_{sj}.

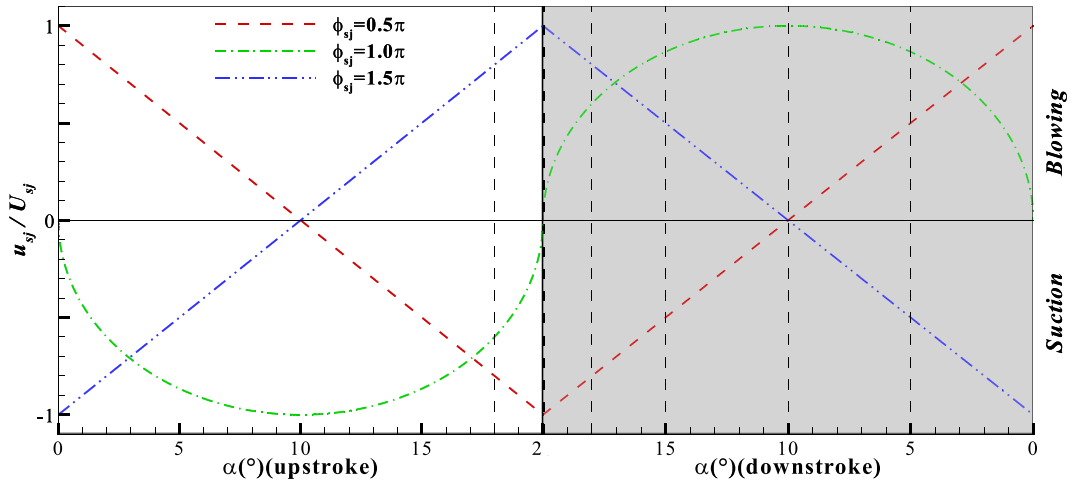

Fig. 7. Angle history of the dimensionless velocity of SJ u_{sj}/U_{sj} with different phase angles ϕ_{sj}. The corresponding vertical dashed lines represent the six instants, $\alpha = 18°\uparrow$, 20° (covered by solid line), $18°\downarrow$, $15°\downarrow$, $10°\downarrow$, and $5°\downarrow$.

marked in Fig. 8. When $\alpha = 18°\uparrow$, Γ_1^- has not been formed and the flow still attaches to the upper surface, as shown in Fig. 8(a1). Therefore, the change of C_L is approximately linear with the increase of the angle of attack before $\alpha = 18°$, as shown in Fig. 9(a). When $\alpha = 20°$, Γ_1^- has already been formed and has detached from the upper surface, which means that the dynamic stall has occurred, as shown in Fig. 8(a2). Thus, C_L starts to decrease before $\alpha = 20°$, as shown in Fig. 9(a). During the downstroke, the clear recirculation region on the upper surface is generated, which then causes the lift reduction and drag increment. Fig. 8(a3–4) indicate that Γ_1^- is moving from the middle to the end of the upper surface, and it finally leaves the airfoil at $\alpha = 10°\downarrow$, as shown in Fig. 8(a5). Therefore, C_L drops clearly compared with that at the same instant $\alpha = 10°\uparrow$ during the upstroke, as shown in Fig. 9(a). Based on the results in Fig. 8(a), it can be inferred that controlling the vortex Γ_1^- can improve the aerodynamic performance, especially at a large angle of attack α. Therefore, the suction or blowing of the SJ can be utilized for the purpose of flow control.

For the controlled case with $\phi_{sj} = 0.5\pi$, the suction time lasts from $10°\uparrow$ to $10°\downarrow$, which can be observed in Fig. 7. Hence, the SJ holds the vortex Γ_1^- at the middle of the upper surface, as shown in Fig. 8(b2–5). This vortex corresponds to a low pressure region; thus, the surrounding flow is absorbed. Consequently, extra lift can be produced, even during the upstroke, where the stall occurs at a large α in the static case. Therefore, the change of C_L is approximately linear with the increase of α during the suction time from $10°\uparrow$ to $10°\downarrow$, as shown in Fig. 9(a). Coincidentally, the suction time just covers the time period with a large α at $\phi_{sj} = 0.5\pi$. Moreover, compared with the uncontrolled case, the C_D is greatly reduced during the suction time, as demonstrated in Fig. 9(b), especially during the downstroke. As shown in Fig. 8 (b1–5), the flow field is nearly unchanged because of the attachment of Γ_1^-. Another potential reason is that the suction jet together with Γ_1^- induces the streamlines to be close to the upper surface of the airfoil, which delays the flow separation. Hence, C_D is decreased greatly during this time period. As α further decreases, the suction converts to blowing, which rapidly destroys the drag reduction and causes the drag to increase. The vortex Γ_1^- moves to the trailing edge quickly, as shown in Fig. 8(b6). C_L first drops slowly before $\alpha = 5°\downarrow$ and then drops very quickly because of the detachment of Γ_1^-. Although the aerodynamic performance is poor when α is small, it is found that the time-averaged lift coefficient is the largest and the time-averaged drag coefficient is the smallest among all the controlled cases considered.

When the phase angle of SJ is $\phi_{sj} = 1.0\pi$, the suction time occurs during the upstroke period while the blowing time occurs during the downstroke period. Because of the upward movement

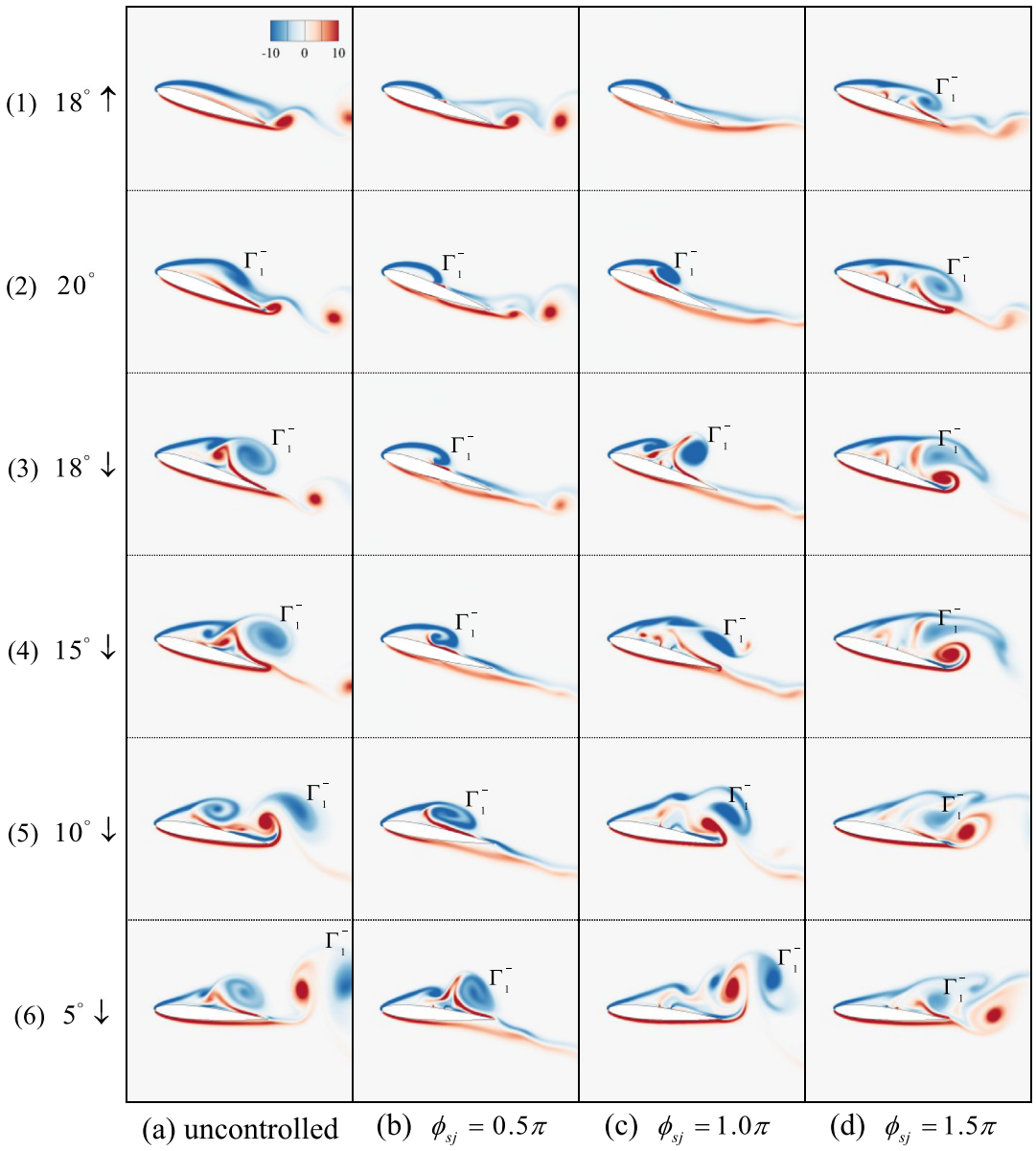

Fig. 8. Vorticity contours around the airfoil at six instants, and the arrows represent the pitching direction, upstroke or downstroke. The results of the uncontrolled case and the 3 cases with different phase angles are compared.

of the pithing airfoil and the suction of the SJ during the upstroke, the fluid attaches to the upper surface tightly and the change of C_L is similar to that of the controlled case with $\phi_{sj} = 0.5\pi$, as shown in Figs. 8(c1) and 9(a). However, the C_L trend is similar to that of the uncontrolled case and drops greatly during the whole downstroke. The vortex Γ_1^- detaches from the upper surface and becomes slender at a large α, as shown in Fig. 8(c2–4). That is the reason why the C_L is reduced compared with that during the upstroke. Although the blowing time covers the whole downstroke, the suction affects the fluid at the large α of the upstroke end and the lagging effect influences the fluid during the downstroke. Hence, the $\overline{C_L}$ is still larger than that of the uncontrolled case. In addition, the C_D is reduced obviously at the large α of the upstroke end, and the principle is similar to that of the case $\phi_{sj} = 0.5\pi$ at the large α of the downstroke beginning, which is plotted in Fig. 9(b). However, the blowing time also enlarges the recirculation region, as shown in Fig. 8 (c3–6), and then it produces a higher drag. Finally, there is little difference in the $\overline{C_D}$ values of this controlled case and the uncontrolled case.

For the controlled case with $\phi_{sj} = 1.5\pi$, the blowing time is in the range from 10°↑ to 10°↓, which is completely opposite to the case of $\phi_{sj} = 0.5\pi$. Therefore, the controlled effect may be opposite. As shown in Fig. 8(d1), the vortex Γ_1^- has been formed during the upstroke, which means that the dynamic stall occurs earlier in this case than in the uncontrolled case. Then, C_L is smaller at $\alpha = 20°$, as shown in Fig. 9(a). During the downstroke from 20° to 10°↓, the C_L is reduced greatly and it becomes slightly negative. The explanation can be found in Fig. 8(d2–6), which demonstrates the detachment of Γ_1^- from the upper surface and the formation of a large recirculation region. However, the C_D is greatly decreased compared with that of the uncontrolled case, as shown in Fig. 9(b). The main reason is also attributed to Γ_1^-, which dominates the flow attachment. Although the vortex Γ_1^- seems to leave the upper surface of the airfoil, the SJ retains it on the airfoil surface at $\alpha = 10°\downarrow$ because suction begins, as shown in Fig. 8 (d5–6). The position of Γ_1^- in Fig. 8(d6) is very different from that in Fig. 8(a6 or c6). Hence, the C_D value is smaller compared with those of the other cases after $\alpha = 10°\downarrow$. It

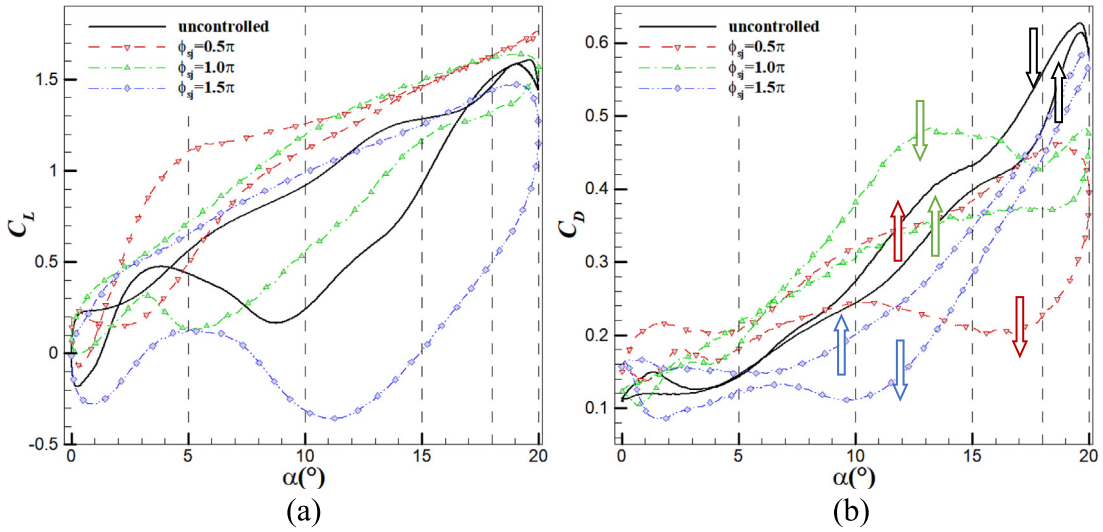

Fig. 9. Comparison of C_L and C_D with different phase angles.

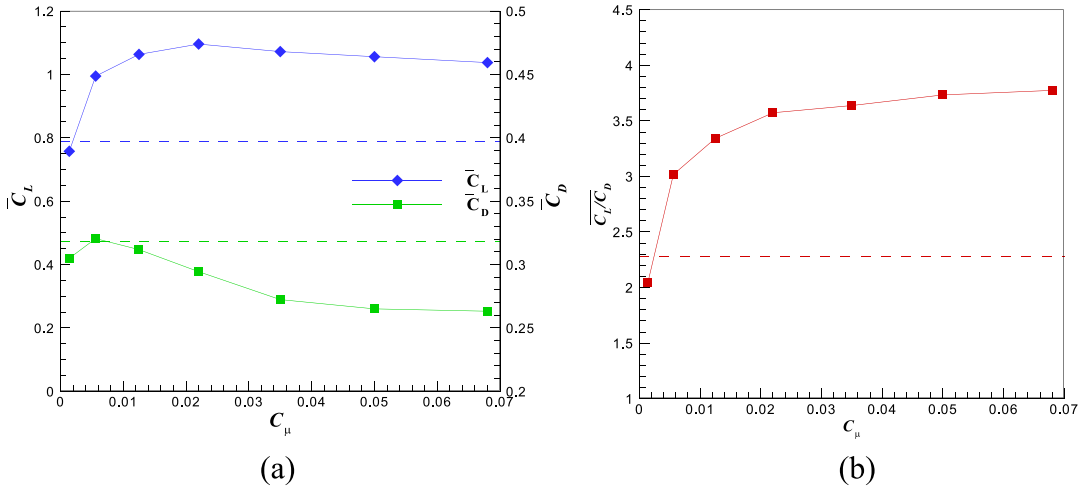

Fig. 10. Time-averaged (a) lift and drag coefficients ($\overline{C_L}$ and $\overline{C_D}$) and (b) the ratio of the lift coefficient to the drag coefficient ($\overline{C_L/C_D}$) varying with the SJ momentum coefficient C_μ.

can be concluded that this phase angle is better for drag reduction but worse for lift increment.

Based on the results in Figs. 6–9, it is clear that the best phase angle is $\phi_{sj} = 0.5\pi$, which obtains the best aerodynamic performance among these controlled cases. Controlling the position of vortex Γ_1^- is very important because it influences the following vortices, which are directly associated with the dynamic stall. Therefore, it is necessary to control the operation time of the suction and blowing of the SJ. From the investigation in this section, it is known that turning on the suction at a large angle of attack can obtain the best lift increment and drag reduction.

3.3. Effect of the jet momentum coefficient

In addition to the jet phase angle, it is also necessary to investigate the effect of the jet momentum coefficient C_μ. Zhao et al. [14] indicated that a larger momentum coefficient could significantly improve the aerodynamic characteristics of the airfoil. However, their SJ control principle is different from the present work; the purpose of their SJ control was to blow the vortices away from the airfoil surface instead of handling the main vortex Γ_1^-. Although a small jet momentum coefficient ($C_\mu = 0.068$ in previous section) is employed in the current study, it is noted that such a coefficient still works well for the compressible flow considered. In this section, seven cases are investigated, where $C_\mu = 0.0014$, 0.0056, 0.0125, 0.022, 0.035, 0.05, and 0.068 ($U_{sj} = 0.125$, 0.25, 0.375, 0.5, 0.625, 0.75, $0.875U_\infty$, respectively). Meanwhile, $H = 0.1c$ with $L = 0.5c$ are chosen in all the cases. In addition, the phase angle with $\phi_{sj} = 0.5\pi$ is used.

Fig. 10 shows the time-averaged lift coefficient, drag coefficient and the ratio of the lift coefficient to the drag coefficient varying with the SJ momentum coefficient C_μ from 0.0014 to 0.068. As in Fig. 6, the results without control, which are denoted as dashed lines, are also included. When the value of C_μ is small, the changes of $\overline{C_L}$, $\overline{C_D}$ and $\overline{C_L/C_D}$ are drastic. However, the variation slope becomes gentle after $C_\mu = 0.035$.

Similar to Fig. 8, the vorticity contours around the airfoil with different momentum coefficients are drawn in Fig. 11. From Fig. 11(b), it seems that the strength of the SJ is too small to handle the vortex Γ_1^- at $C_\mu = 0.0056$. The constraint on Γ_1^- is not enough and its growth and detachment are earlier than in the case with $C_\mu = 0.068$ during the whole pitching period. The vortex Γ_1^- is far away from the airfoil at $\alpha = 5°\downarrow$, as shown in Fig. 11(b6). Hence, the increment of $\overline{C_L}$ and the reduction of $\overline{C_D}$ are not satisfactory at $C_\mu = 0.0056$. However, when C_μ increases from 0.035 to 0.068, the discrepancies of the flow patterns around

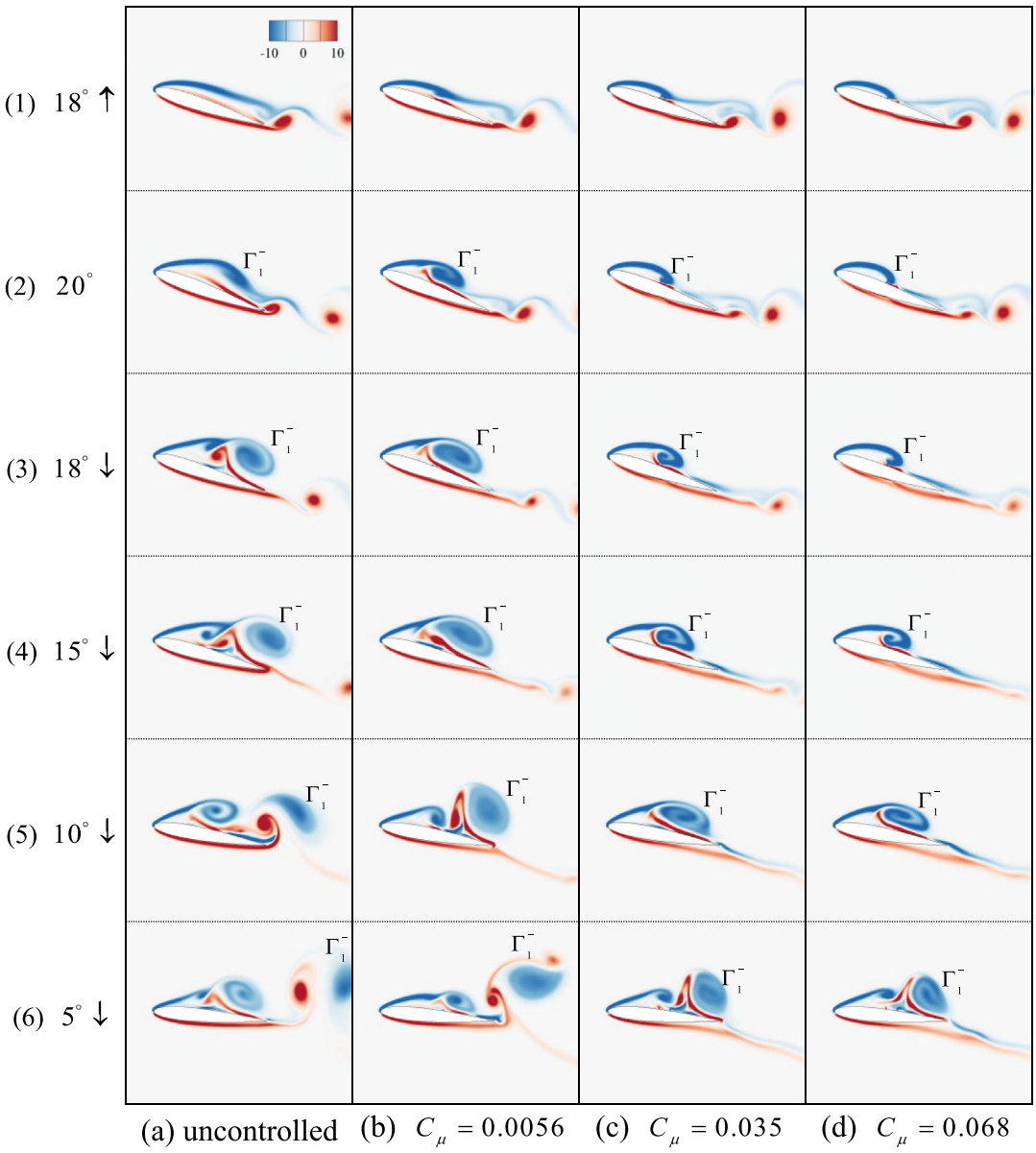

Fig. 11. Vorticity contours around the airfoil at six instants, and the arrows represent the pitching direction, upstroke or downstroke. The results of the uncontrolled case and the 3 cases with different momentum coefficients are compared.

the airfoil are not obvious during the whole pitching period, as shown in Fig. 11(c) and (d). Therefore, the aerodynamic characteristics of the pitching airfoil cannot be improved significantly by increasing the momentum coefficient after $C_\mu = 0.035$. Except at a very small C_μ, a variation in C_μ does not have a large influence on the aerodynamic performance, which means that once the amplitude of the jet velocity is large enough to handle the vortex Γ_1^-, it is not advisable to further increase the momentum coefficient. Thus, $C_\mu = 0.035$ ($U_{sj} = 0.625U_\infty$) might be a good choice in the present work, as it is not only able to obtain a satisfactory aerodynamic performance but can also save the energy of the SJ.

3.4. Effect of jet location

After the jet phase angle and momentum coefficient, the influence of the location of the jet center is also investigated. Five SJ locations ($L = 0.3c$, $0.4c$, $0.5c$, $0.6c$, and $0.7c$) are selected. The other SJ control parameters are chosen as follows: $C_\mu = 0.068$ ($U_{sj} = 0.875U_\infty$ and $H = 0.1c$) and $\phi_{sj} = 0.5\pi$.

Fig. 12 shows the time-averaged lift coefficient, drag coefficient and the ratio of the lift coefficient to the drag coefficient varying with the location of the jet center. As the jet location moves back to the trailing edge of the airfoil, both $\overline{C_L}$ and $\overline{C_D}$ increase. However, $\overline{C_L/C_D}$ gradually decreases. Again, the vorticity contours around the airfoil with different jet locations are presented in Fig. 13. From this figure, it is easy to find that the vortex Γ_1^- is held at the jet center for every controlled case. Furthermore, the size of Γ_1^- increases when the jet location moves back to the trailing edge of the airfoil. A possible reason is that the vortex Γ_1^- is formed near the leading edge and the earlier control can restrain its growth. When the jet center is very close to the trailing edge, however, a clear negative pressure region is produced because of the circulation of vortex Γ_1^-. Then, it produces an extra force along the upper right direction on the upper surface of the airfoil. This additional force can enhance both $\overline{C_L}$ and $\overline{C_D}$. Therefore, the location of the jet center being away from the leading edge can increase both the lift and drag coefficients. However, the lift–drag ratio decreases. When the jet

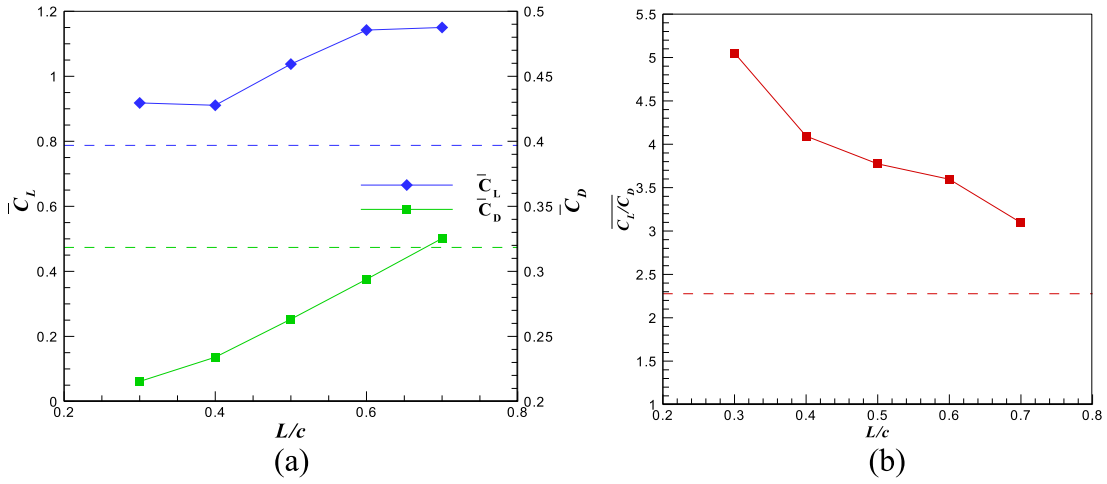

Fig. 12. Time-averaged (a) lift and drag coefficients ($\overline{C_L}$ and $\overline{C_D}$) and (b) the ratio of the lift coefficient to the drag coefficient ($\overline{C_L/C_D}$) varying with the location of jet center.

Table 2
Comparison of the time-averaged lift and drag coefficients with and without synthetic jet control at different Mach numbers. The synthetic jet parameters are set to $C_\mu = 0.068$ ($U_{sj} = 0.875U_\infty$, $H = 0.1c$), $\phi_{sj} = 0.5\pi$ and $L = 0.5c$.

Case	Coefficient	Uncontrolled	SJ control	Increment
$Ma = 0.2$	$\overline{C_L}$	0.7326	0.9790	33.6%
	$\overline{C_D}$	0.2983	0.2415	−19.0%
	$\overline{C_L/C_D}$	2.1159	4.1523	96.2%
$Ma = 0.4$	$\overline{C_L}$	0.7875	1.0375	31.8%
	$\overline{C_D}$	0.3184	0.2632	−17.3%
	$\overline{C_L/C_D}$	2.2769	3.7741	65.8%

Table 3
Comparison of the time-averaged lift and drag coefficients with and without synthetic jet control at different Mach numbers. The synthetic jet parameters are set to $C_\mu = 0.035$ ($U_{sj} = 0.625U_\infty$, $H = 0.1c$), $\phi_{sj} = 0.5\pi$ and $L = 0.5c$.

Case	Coefficient	Uncontrolled	SJ control	Increment
$Ma = 0.2$	$\overline{C_L}$	0.7326	0.9442	28.9%
	$\overline{C_D}$	0.2983	0.2401	−19.5%
	$\overline{C_L/C_D}$	2.1159	3.7915	79.2%
$Ma = 0.4$	$\overline{C_L}$	0.7875	1.0722	36.2%
	$\overline{C_D}$	0.3184	0.2724	−14.5%
	$\overline{C_L/C_D}$	2.2769	3.6382	59.8%

position is advanced, the vortex Γ_1^- can be controlled earlier, and the unstable recirculation region of the airfoil upper surface is smaller. It can be concluded that better aerodynamic performance can be obtained by placing the jet at the leading edge.

3.5. Effect of compressibility

To apply jet control to the thin Martian atmosphere, the impact of the compressibility of the gas on the control effect must be considered. The Mach number in the above sections is set to 0.4, and this section will be set to 0.2. First, the same synthetic jet parameters as in Section 3.1 will be applied. A synthetic jet with $C_\mu = 0.068$ ($U_{sj} = 0.875U_\infty$, $H = 0.1c$), $\phi_{sj} = 0.5\pi$ and $L = 0.5c$ is added to the upper surface of the airfoil.

Fig. 14 shows the vorticity contours with different Mach numbers. Since the difference is not large, only the results at three moments are given. It can be seen that when the Mach number is low, the unstable region and the vortex Γ_1^- are smaller, which means that the control effect is better. Table 2 shows $\overline{C_L}$, $\overline{C_D}$ and $\overline{C_L/C_D}$ with different Mach numbers. When the Mach number is increased from 0.2 to 0.4, the effects of increasing lift and reducing drag due to jet control are reduced. The time-averaged lift-to-drag ratio improvement effect is reduced by nearly 30%. It is mentioned in Section 3.3 that the momentum coefficient of the jet is not as large as is possible, and an excessively large momentum coefficient does not greatly improve the control effect. Therefore, another set of jets will use the appropriate momentum coefficient $C_\mu = 0.035$ ($U_{sj} = 0.625U_\infty$, $H = 0.1c$, recommended values in Section 3.3). As in Tables 2, 3 also gives $\overline{C_L}$, $\overline{C_D}$ and $\overline{C_L/C_D}$. It can also be found that when the Mach number is increased, the improvement effect of the jet on aerodynamic performance is reduced. In particular, the increasing amount of $\overline{C_L}$ is better when the Mach number is larger. It can be concluded that the higher the Mach number, the worse the jet control effect.

4. Conclusions

In this study, a synthetic jet is employed to control the dynamic stall and improve the aerodynamic performance of a pitching NACA0012 airfoil in a low Reynolds number compressible flow, which can be operated in the Martian atmosphere. A variable correction-based immersed boundary method developed in a previous work [17] is adopted to conduct the numerical simulations. After the validation of the numerical method for the dynamic stall problem, systematic investigations are carried out. The main findings are as follows.

1. The phase angle ϕ_{sj} is an important parameter. The aerodynamic performance of the airfoil could be greatly affected by the choice of ϕ_{sj}. The main vortex Γ_1^- almost dominates the flow on the upper surface of the airfoil. Choosing its position and growth appropriately are the crucial points to control the dynamic stall. Controlling the suction and blowing time of the SJ can effectively operate the vortex Γ_1^-. It is useful to adjust the phase angle for triggering the suction time of the SJ at large angle of attack, which can produce the best lift increment and drag reduction.
2. The momentum coefficient C_μ is small in the present work and can also achieve a satisfactory SJ control result. Increasing the C_μ can improve the aerodynamic characteristics of the airfoil because a stronger SJ can handle the vortex Γ_1^- better. Nevertheless, when the C_μ is higher than some

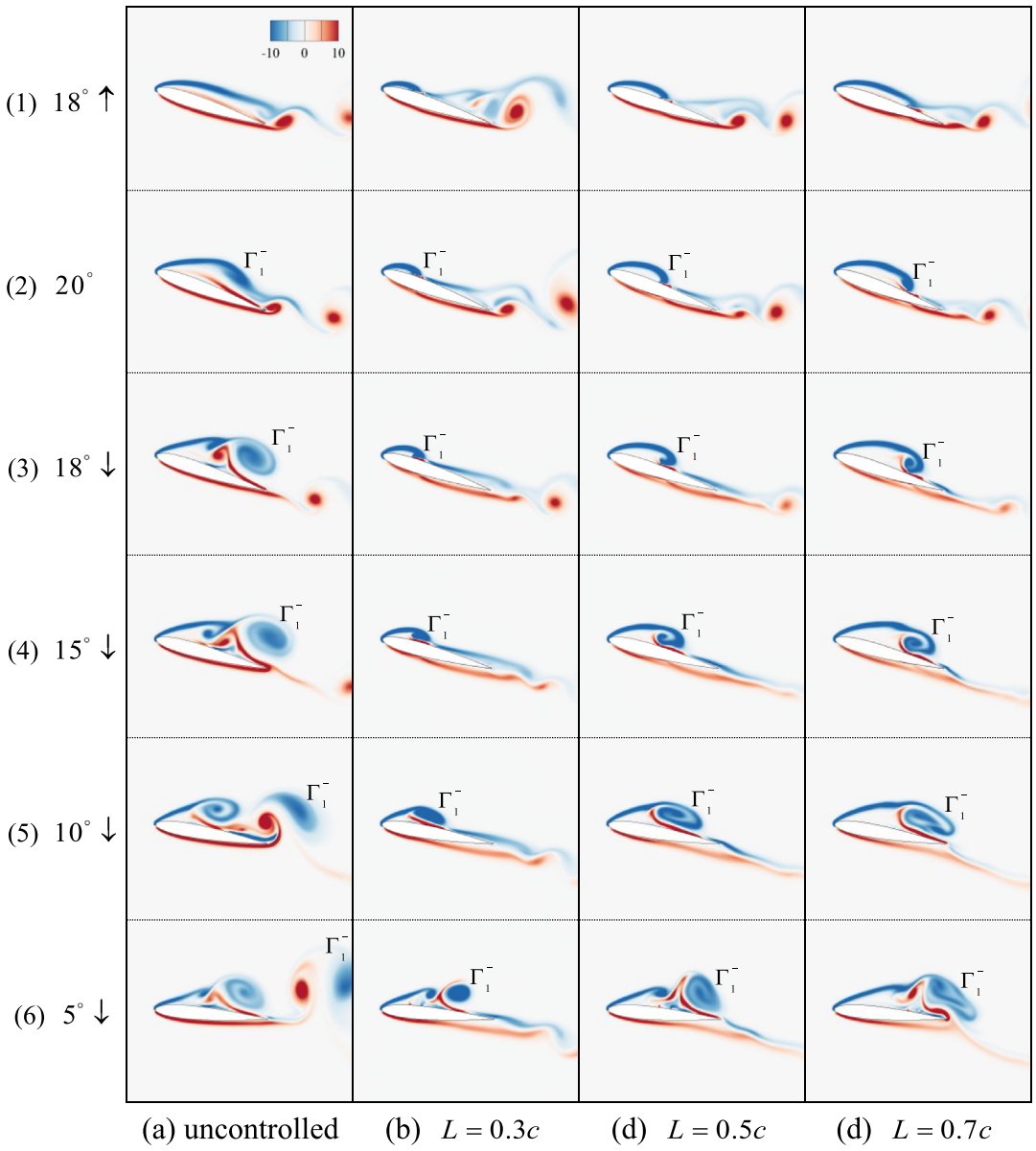

Fig. 13. Vorticity contours around the airfoil at six instants, and the arrows represent the pitching direction, upstroke or downstroke. The results of the uncontrolled case and the 3 cases with different locations of the jet center are compared.

fixed value, the improvement becomes weak. Generally speaking, an appropriate C_μ value is suggested rather than a stronger value.

3. The location of the jet center L is also an important parameter in the SJ control. A small value of L can control the vortex earlier and restrain the vortex's growth and vice versa. A larger vortex Γ_1^- produces not only a larger lift but also a larger drag. However, in general, placing the jet at the leading edge is more conducive to improving the aerodynamic performance.
4. The compressibility of the fluid also affects the effectiveness of the SJ control. The higher the Mach number, the worse the SJ control effect will be.

The efficiency of the synthetic jet control for the dynamic stall is related to the proper choice of parameters, such as the phase angle, the momentum coefficient and the location of the jet center. In addition, the flow field environment will also affect the control effect. On the other hand, other parameters, such as the jet angle, can also influence the control efficiency. In the future work, more parametric analyses will be performed. Furthermore, the dynamic stall of the pitching airfoil will be controlled in a high Reynolds number flow.

Declaration of competing interest

The authors declare that they have no known competing financial interests or personal relationships that could have appeared to influence the work reported in this paper.

Acknowledgments

J. W. acknowledges the support of the National Natural Science Foundation of China (Grant Nos. 11622219, 11772157) and the Natural Science Foundation of Jiangsu Province, China (Grant

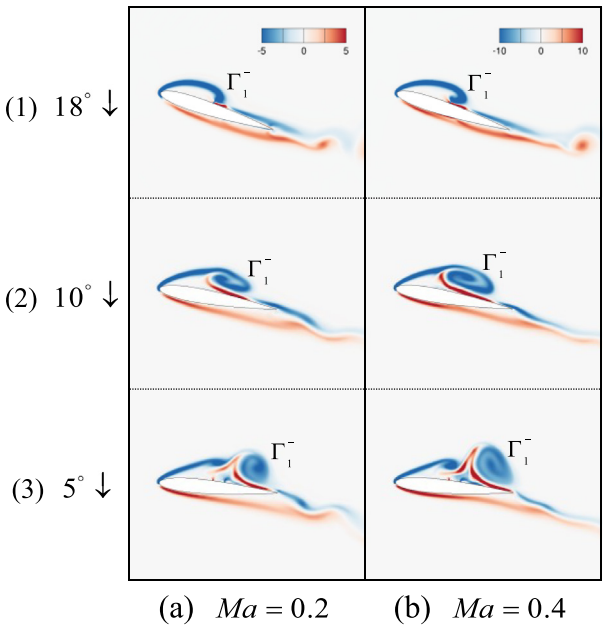

Fig. 14. Vorticity contours around the airfoil at three instants, and the arrows represent the pitching direction, upstroke or downstroke. The results in two different flow fields (different Mach numbers) but with the same SJ are compared.

No. BK20191271). This work is also supported by the Priority Academic Program Development of Jiangsu Higher Education Institutions (PAPD), China.

References

[1] T. Désert, T. Jardin, H. Bézard, J.M. Moschetta, Numerical predictions of low Reynolds number compressible aerodynamics, Aerosp. Sci. Technol. 92 (2019) 211–223.
[2] P.M. Munday, K. Taira, T. Suwa, D. Numata, K. Asai, Nonlinear lift on a triangular airfoil in Low-Reynolds-Number compressible flow, J. Aircr. 52 (3) (2015) 924–931.
[3] C.C. Tseng, Y.E. Cheng, Numerical investigations of the vortex interactions for a flow over a pitching foil at different stages, J. Fluids Struct. 58 (2015) 291–318.
[4] H.R. Karbasian, K.C. Kim, Numerical investigations on flow structure and behavior of vortices in the dynamic stall of an oscillating pitching hydrofoil, Ocean Eng. 127 (2016) 200–211.
[5] K.W. McAlister, L.W. Carr, W.J. McCroskey, Dynamic stall experiments on the NACA 0012 airfoil, in: NASA Technical Paper 1100, 1978.
[6] W.J. McCroskey, L.W. Carr, K.W. McAlister, Dynamic stall experiments on oscillating airfoils, AIAA J. 14 (1976) 57–63.
[7] M.R. Visbal, Analysis of the onset of dynamic stall using high-fidelity Large-Eddy Simulations, in: 52nd Aerospace Sciences Meeting, AIAA 2014-0591.
[8] M.R. Visbal, Dynamic stall of a constant-rate pitching airfoil, J. Aircr. 27 (1990) 400–407.
[9] W.H. Guo, D.X. Fu, Y.W. Ma, Numerical investigation of dynamic stall of an oscillation aerofoil, Internat. J. Numer. Methods Fluids 19 (1994) 723–734.
[10] Y.Y. Niu, C.C. Chang, How do aerodynamic forces of the pitching rigid and flexible airfoils evolve? AIAA J. 51 (2013) 2946–2952.
[11] J. Zhong, J. Li, P. Guo, Y. Wang, Dynamic stall control on a vertical axis wind turbine aerofoil using leading-edge rod, Energy 174 (2019) 246–260.
[12] W. Geissler, B.G. van der Wall, Dynamic stall control on flapping wing airfoils, Aerosp. Sci. Technol. 62 (2017) 1–10.
[13] Z.L. Tang, J.D. Sheng, G.D. Zhang, J. Periaux, Large-scale separation flow control on airfoil with synthetic jet, Int. J. Comput. Fluid Dyn. 32 (2018) 104–120.
[14] Q. Zhao, Y. Ma, G. Zhao, Parametric analyses on dynamic stall control of rotor airfoil via synthetic jet, Chin. J. Aeronaut. 30 (2017) 1818–1834.
[15] C. Wang, H. Tang, F. Duan, S.C.M. Yu, Control of wakes and vortex-induced vibrations of a single circular cylinder using synthetic jets, J. Fluids Struct. 60 (2016) 160–179.
[16] C. Wang, H. Tang, Enhancement of aerodynamic performance of a heaving airfoil using synthetic-jet based active flow control, Bioinspiration Biomim. 13 (2018) 046005.
[17] J. Wang, Y. Li, J. Wu, F. Qiu, A variable correction-based immersed boundary method for compressible flows over stationary and moving bodies, Adv. Appl. Math. Mech. 12 (2020) 545–563.
[18] Y.L. Qiu, C. Shu, J. Wu, Y. Sun, L.M. Yang, T.Q. Guo, A boundary condition-enforced immersed boundary method for compressible viscous flows, Comput. & Fluids 136 (2016) 104–113.
[19] M.R. Visbal, R.E. Gordnier, M.C. Galbraith, High-fidelity simulations of moving and flexible airfoils at low reynolds numbers, Exp. Fluids 46 (2009) 903–922.